International Journal of Multiphysics
Volume 18, No. 2, 2024
ISSN: 1750-9548

A Station Selection Model Considering Intra-board Deformation and Strain Visualization Analysis

Chengcheng Fan*, Jintong Ren, Zhihong Wang, ChunXia Wang, Hui Wang
College of Mining Engineering, Guizhou University of Engineering Science, China
*Corresponding Author.

Abstract

Computer visualization can intuitively reflect the process and results of crustal deformation. In this paper, taking into account the intraplate deformation, combined with computer visualization technology, using robust estimation method that can identify data with high collapse pollution rate, combined with the overall rotation and linear strain model (RELSM) that describes block movement, the GPS observation velocity field data of the Chinese Mainland tectonic environment monitoring network located in Ordos and its adjacent areas are screened, and the strain data are calculated to generate visual images for analysis. The results show that the method proposed in this paper can effectively consider the smoothness of internal plate deformation and the differences in local structures, suppress gross errors, and obtain good velocity field fitting results.

Keywords: Crustal deformation, station selection, robust estimation, strai, visualization analysis.

1. Introduction

With the development of Earth sciences, increasing attention has been drawn to the study of crustal deformation. Crustal deformation, which involves changes in the Earth's surface or subsurface structures, often accompanies natural disasters such as earthquakes and volcanic activities, profoundly impacting human society. In order to better understand and predict the processes and mechanisms of crustal deformation, scientists utilize computer visualization techniques to transform complex geological data into intuitive images for analysis and research. Through visualization, we can observe deformation patterns on the Earth's surface, changes in subsurface structures, and trends in crustal movements, providing important insights for the prevention and mitigation of geological hazards. This paper explores the application of computer visualization in the study of crustal deformation, as well as its significance and potential directions for development in the field of Earth sciences.

Research indicates that crustal movements exhibit viscoelastic deformation [1-3]. Crustal movements induce horizontal and vertical deformations on the Earth's surface and within its interior. However, due to the influence of local structural differences in the blocks and observation outliers, a small number of stations often exhibit anomalous movements, also known as outlier stations. Strictly speaking, the anomalous movements of stations caused by tectonic forces are very complex and fundamentally different from the nature of observation outliers. However, they objectively reflect the actual motion trends of the stations. Therefore, when screening for anomalous stations in block movements, these anomalies cannot simply be treated as outliers; instead, their impact on actual motion should be considered, taking into account the smoothness of intra-block deformation [4-6].

Currently, models used to study block movements mostly regard block movements as rigid. Due to the stable long-term trends in their movements, it is believed that there is no deformation inside the blocks or that deformation only occurs within certain belt ranges at the edges of the blocks. Therefore, for the removal of outlier stations, most methods are based on twice the residual standard deviation of the fitting of rigid movement as the threshold for judgment and removal. This method assumes that stations deviating from the overall

movement trend contain outliers. However, when intra-block deformation is inconsistent with the overall trend of movement, the removal of outlier stations must consider local block structures. Therefore, the selection of outlier stations should consider intra-block deformation while also considering the influence of outliers, adopting robust measures to rationalize station removal and make velocity field models more realistic.

In this paper, intra-block deformation is considered. Robust estimation methods capable of identifying data with high breakdown pollution rates [7-9] are used, combined with a model describing the overall rotation and linear strain of block movements (Rotation Entirety and Linear Strain Model). This approach is applied to the GPS observation velocity field data from the mainland China structural environmental monitoring network in the Ordos and its neighboring areas for station selection, fitting, and strain calculation. The results outperform those of the robust rigid model for station selection, and the strain analysis also aligns with reality.

2. Block Movement Model

2.1 Rigid Body Movement Model (RRM)

The mathematical model of rigid body motion according to Euler's theorem is as follows:

$$\boldsymbol{V} = \boldsymbol{\Omega} \times \boldsymbol{R} \tag{1}$$

In the equation, $\boldsymbol{V}$ represents the velocity of rigid body motion, $\boldsymbol{\Omega}$ denotes the Euler vector of the rigid body, and $\boldsymbol{R}$ stands for the position vector from a point on the rigid body to the center of motion.

When the purpose is to quantitatively understand or grasp the overall movement of the regional crust, block movement is often considered as rigid motion. Based on Euler's theorem, horizontal crustal movement is equivalently represented as finite rotational motion about the Euler axis. Therefore, assuming in a Cartesian coordinate system centered at the Earth's center, the absolute Euler vector $\boldsymbol{\Omega}(\omega_x, \omega_y, \omega_z)$ and the motion radius $\boldsymbol{R}(x, y, z)$ of a certain block are known, then according to equation (1), the expression for the rigid motion velocity $\boldsymbol{V}_{\mathrm{g}}(v_x, v_y, v_z)$ of a point on this block is given by:

$$\begin{bmatrix} V_x \\ V_y \\ V_z \end{bmatrix} = \begin{bmatrix} 0 & z & -y \\ -z & 0 & x \\ y & -x & 0 \end{bmatrix} \begin{bmatrix} \omega_x \\ \omega_y \\ \omega_z \end{bmatrix} \tag{2}$$

By considering the transformation relationship between the Cartesian coordinate system centered at the Earth's center and the spherical geographic coordinate system, equation (2) can be converted to:

$$\begin{bmatrix} V_x \\ V_y \\ V_z \end{bmatrix} = \begin{bmatrix} 0 & r\sin\varphi & -r\cos\varphi\sin\lambda \\ -r\sin\varphi & 0 & r\cos\varphi\cos\lambda \\ r\cos\varphi\sin\lambda & -r\cos\varphi\cos\lambda & 0 \end{bmatrix} \begin{bmatrix} \omega_x \\ \omega_y \\ \omega_z \end{bmatrix} \tag{3}$$

In the equation, λ and φ represent the geodetic longitude and geodetic latitude, respectively, of a point on the block. Since the velocity field values obtained from actual observations are generally ground station velocities, the Earth-centered velocity in equation (3) should be converted to station-centered velocity. This conversion involves transforming V_x, V_y, V_z into V_e, V_n, V_h, and the transformation relationship is as follows:

$$\begin{bmatrix} V_e \\ V_n \\ V_h \end{bmatrix} = \begin{bmatrix} -\sin\lambda & \cos\lambda & 0 \\ -\sin\varphi\cos\lambda & -\sin\varphi\sin\lambda & \cos\varphi \\ \cos\varphi\cos\lambda & \cos\varphi\sin\lambda & \sin\varphi \end{bmatrix} \begin{bmatrix} V_x \\ V_y \\ V_z \end{bmatrix} \tag{4}$$

When studying the movement of crustal plates, vertical motion is often disregarded, with the assumption that plate movement primarily occurs in its horizontal direction. Therefore, equations (4) and (3) yield:

$$\begin{bmatrix} V_e \\ V_n \end{bmatrix} = \begin{bmatrix} -r\cos\lambda sin\varphi & -r\sin\lambda\sin\varphi & r\cos\varphi \\ \sin\lambda & -r\cos\lambda & 0 \end{bmatrix} \begin{bmatrix} \omega_x \\ \omega_y \\ \omega_z \end{bmatrix} \tag{5}$$

Equation (5) represents the rigid motion model of the block. The establishment of the rigid motion model has greatly promoted the development of crustal movement. According to the above equation, if the station-centered position and Euler rotation vector on the block are known, the corresponding velocity of the station center can be obtained, allowing for the generation of velocity field images for the block. Conversely, if a certain number of station-centered velocities and positions on a block can be observed, the Euler vector can be inverted based on specific mathematical principles, further enabling the determination of the block's angular velocity of rotation and Euler pole coordinates. In geosciences, l typically represents the longitude corresponding to the geographic coordinates of the Euler pole, φ represents latitude, and $\boldsymbol{\omega}$ represents the angular velocity of rotation about the Euler axis. They are related by the following equations:

$$\begin{cases} \boldsymbol{\omega} = \sqrt{\omega_x^2 + \omega_y^2 + \omega_z^2} \\ l = \arctan\left(\dfrac{\omega_y}{\omega_x}\right) \\ \varphi = \arctan\left(\dfrac{\omega_z}{\sqrt{\omega_x^2 + \omega_y^2}}\right) \end{cases} \tag{6}$$

The relationship between the Euler vector $\boldsymbol{\Omega}(\omega_x, \omega_y, \omega_z)$ and the angular velocity of Euler motion $\boldsymbol{\omega}$ can be expressed as:

$$\begin{cases} \omega_x = \boldsymbol{\omega}\cos\varphi\cos\lambda \\ \omega_y = \boldsymbol{\omega}\cos\varphi\sin\lambda \\ \omega_z = \boldsymbol{\omega}\sin\varphi \end{cases} \tag{7}$$

2.2 Rotation Entirety and Linear Strain Model (RELSM)

Extensive research has shown that when a block is subjected to external forces, it undergoes a certain degree of deformation locally, and the motion of a point should be a composite of the block's overall rigid rotational motion and local viscoelastic deformation. Assuming that the deformation inside the block is uniform, the following model of overall rotation and uniform strain (REHSM) can be proposed [10~18]:

$$\begin{bmatrix} \boldsymbol{V}_e \\ \boldsymbol{V}_n \end{bmatrix} = r \begin{bmatrix} -\cos\lambda\sin\varphi & -\sin\lambda\sin\varphi & \cos\varphi \\ \sin\lambda & -\cos\varphi & 0 \end{bmatrix} \begin{bmatrix} \omega_x \\ \omega_y \\ \omega_z \end{bmatrix} + \begin{bmatrix} \varepsilon_e & \varepsilon_{en} \\ \varepsilon_{ne} & \varepsilon_n \end{bmatrix} \begin{bmatrix} x \\ y \end{bmatrix} \tag{8}$$

where λ_0, φ_0 represents the strain parameter; x, y are the coordinates of the spherical coordinate system, determined by the following equation:

$$\left.\begin{aligned} x &= r(\lambda - \lambda_0)\cos\varphi \\ y &= r(\varphi - \varphi_0) \end{aligned}\right\} \tag{9}$$

In the equation, (λ_0, φ_0) represents the central longitude and latitude of the region, and the meanings of other parameters are the same as in equation (5). If it is further assumed that the deformation inside the block varies linearly, the model of the overall rotation and linear strain of crustal movement (RELSM) can be obtained:

$$\begin{bmatrix} \boldsymbol{V}_s \end{bmatrix} \quad \begin{bmatrix} \end{bmatrix} \begin{bmatrix} \boldsymbol{\omega}_y \end{bmatrix} + \begin{bmatrix} \end{bmatrix} \begin{bmatrix} y \end{bmatrix} - \begin{bmatrix} \end{bmatrix} \begin{bmatrix} \ _2 \end{bmatrix} + \begin{bmatrix} \end{bmatrix} xy \tag{10}$$

In the above equation, $A_0 \sim A_2$, $B_0 \sim B_2$, $C_0 \sim C_2$ all represent strain parameters.

Both of the aforementioned models consider the overall movement trend of the plates while also reflecting the internal deformation characteristics of the plates, resulting in a higher precision in velocity field fitting compared to RRM. However, REHSM considers intra-block deformation as uniform strain, which does not align with the actual block structure and is suitable for smaller secondary blocks within a region. On the other hand, RELSM assumes intra-block deformation to be linearly variable, taking into account the diversity of block internal structures, thus being closer to reality and applicable for a broader range of block movement deformation analyses.

3. Robust Estimation Station Selection and Velocity Field Fitting in RELSM

Research has shown that block motion is a combination of overall trend-like rigid motion and irregular internal deformation. When establishing a regional crustal motion deformation analysis model, it is essential to fully consider the long-term stability of overall motion and the local heterogeneity of internal structures within the region's blocks. Therefore, in the selection of station filtering methods, it is necessary to adopt station exclusion methods that simultaneously consider both overall characteristics and local differences to balance the features of the overall and local movements.

Typically, in the absence of outliers, it is assumed that the residual velocity values should follow a normal distribution, and the residual velocities of most stations should fall within a reasonable range. Stations with residual velocities exceeding a certain limit are considered outliers and are removed. If a limit of 2 is chosen, stations with residual velocities greater than 2 are removed. This method treats stations that deviate from the overall trend as outliers, resulting in higher fitting accuracy, but it overlooks the actual impact of internal block differences.

Based on the actual movement of the blocks and combining it with the outlier handling approach, robust estimation using the equivalent weight theory is employed for station selection. Due to the unclear reasons for internal block deformation, dynamic mechanisms, and differences at each point, this paper adopts the high breakdown pollution rate robust estimation method for station selection [2]. The specific steps are as follows:

1) Take the median of all station velocity values, subtract this median from each station velocity value, and obtain the initial residual as:

$$\Delta L_i = L_i - \mathrm{med}(L) \tag{11}$$

Due to the differences in block movement in the east-west direction, it is necessary to calculate the exclusion separately in the eastward and westward directions.

2) Calculate the initial robust estimate of the mean square deviation factor for $\Delta \boldsymbol{L}$:

$$\boldsymbol{\sigma}_{\Delta \boldsymbol{L}} = \mathrm{med}(|\Delta \boldsymbol{L}|)/0.6745 \tag{12}$$

3) Adopting a strong elimination function:

$$P_i^0 = \begin{cases} 1 & |\Delta L_i / \boldsymbol{\sigma}_{\Delta L}| < k_0 \\ 0 & |\Delta L_i / \boldsymbol{\sigma}_{\Delta L}| \geq k_0 \end{cases} \tag{13}$$

In the equation, k_0 is typically chosen empirically as 1.0 or 1.5; in this paper, we set k_0 to 1.5.

4) Using the initial weights, apply RELSM for weighted least squares estimation, obtaining parameter estimates, observation residuals, and variance factors.

$$\begin{cases} \hat{\boldsymbol{X}} = \left(\boldsymbol{A}^{\mathrm{T}} \bar{\boldsymbol{P}}_{\boldsymbol{i}}^{0} \boldsymbol{A}\right)^{-1} \boldsymbol{A}^{\mathrm{T}} \bar{\boldsymbol{P}}_{\boldsymbol{i}}^{0} \boldsymbol{L} \\ \boldsymbol{V} = \boldsymbol{A}\hat{\boldsymbol{X}} - \boldsymbol{L} \\ \boldsymbol{\sigma} = \mathrm{med}\left(|\boldsymbol{V}|\right) / 0.6745 \end{cases} \tag{14}$$

5) Construct equivalent weights using the IGG III weight function:

$$P_{\boldsymbol{i}} = \begin{cases} P_i & \bar{V}_i = \left|\dfrac{V_i}{\boldsymbol{\sigma}}\right| \le k_1 \\ P_i \dfrac{k_1}{\left|\bar{V}_i\right|}\left(\dfrac{k_1 - \left|\bar{V}_i\right|}{k_2 - k_1}\right) & k_1 < \bar{V}_i \le k_2 \\ 0 & \bar{V}_i > k_2 \end{cases} \tag{15}$$

According to empirical evidence, *k1* is typically set between 1.0 and 1.5, while *k2* ranges from 2.5 to 3.0 in the equation. In this paper, we set *k1* to 1.5 and *k2* to 3.0. Substitute equation (15) into equation (10) to solve for the relevant parameters, then repeat steps 4) and 5) ,Stop repeating when the condition is satisfied of $\left|\hat{\boldsymbol{X}}^{k+1} - \hat{\boldsymbol{X}}^{k}\right| < \boldsymbol{\delta}$ ($\boldsymbol{\delta}$ is a minimum value greater than zero; in this paper, we set $\boldsymbol{\delta}$ to be 10^-10). Remove the stations corresponding to equivalent weights of 0, then use the remaining station data for model construction and parameter estimation, and compute the strain.

4. Application and Analysis

This paper utilizes GPS ground observation velocity field data from the China mainland structural environment monitoring network between 2009 and 2014. The GPS station velocities are processed using GAMIT/GLOBK software, resulting in unified velocity field data for the China mainland crust in the ITRF2008 framework, with an accuracy better than 2.5 mm/year [19]. Based on extensive research literature concerning the Ordos region [9-10], the boundaries of the Ordos and its adjacent areas are delineated. A total of 343 station velocity field data points are selected. Figure 1 shows the distribution of stations in the Ordos and its adjacent areas from 2009 to 2014 in the ITRF2008 framework, while Figure 2 depicts the corresponding velocity field image. This image can reflect the spatial distribution of monitoring stations in the study area and the overall trend of crustal movement.

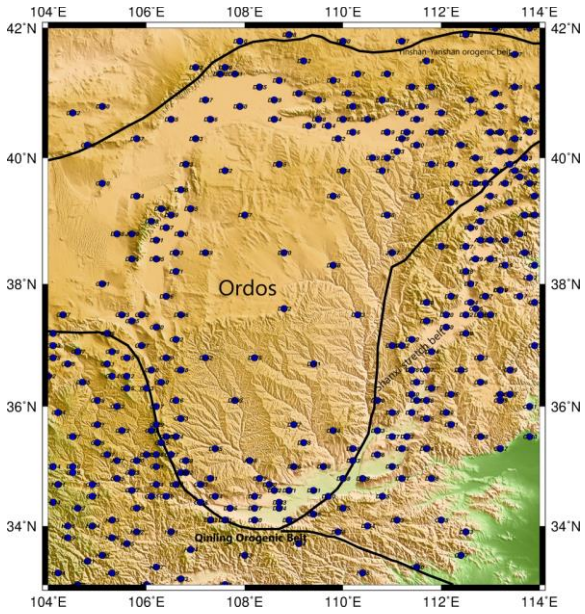

Figure 1 Distribution of monitoring stations in ordos and its adjacent areas

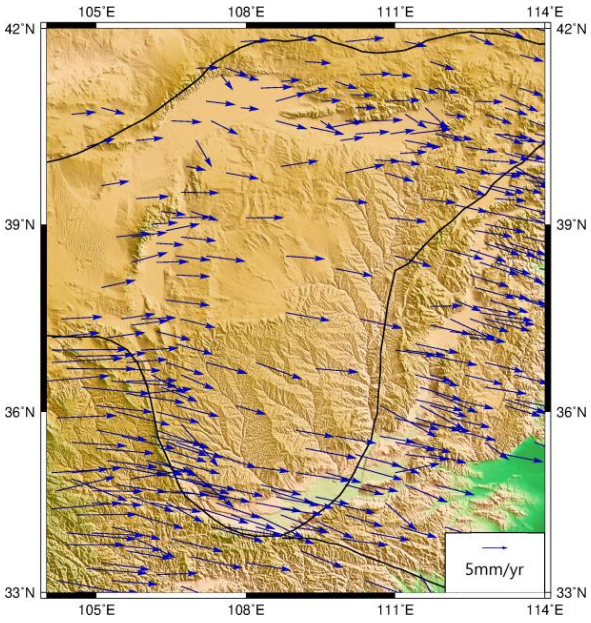

Figure 2 Velocity field in ordos and its adjacent areas

To validate the methodology proposed in this paper, three approaches were employed to conduct station selection and fitting analysis on GPS velocity field data in the Ordos and its adjacent areas.

Approach I: Utilizing the RELSM model to fit the velocity field for all stations and obtain corresponding parameters.

Approach II: Employing the robust estimation of rigid body motion (RRM) model for iterative selection, followed by fitting analysis of RRM velocity field on the selected stations after iteration.

Approach III: Employing the robust estimation of rigid body motion and linear model (RELSM) for iterative selection, followed by fitting analysis of RELSM velocity field on the selected stations after iteration.

The merits of a model are generally assessed through its fitting performance with the data, often measured using statistical principles of unbiasedness and efficiency. Concerning the three aforementioned approaches, their unbiasedness is manifested by the difference between the observed values and the model-adjusted values,

known as the residual mean. A residual mean with an absolute value closer to 0 indicates a better fit. Efficiency, on the other hand, is demonstrated by the dispersion of velocity residuals, i.e., the magnitude of the residual standard deviation. A smaller residual standard deviation indicates higher accuracy. The formulas for calculating the residual mean and the residual standard deviation are as follows:

$$S_{\Delta V}=\left[\frac{1}{2n-r}\left(\sum_{i=1}^{n}\left(\Delta \boldsymbol{V}_{ei}\right)_i^2+\sum_{i=1}^{n}\left(\Delta \boldsymbol{V}_{ni}\right)_i^2\right)\right]^{\frac{1}{2}} \tag{16}$$

In the context, $\Delta V_{ei}, \Delta V_{ni}$ denotes the residuals of the movement velocities of the i^{th} station in the east-west and north-south directions, with r representing an unknown number of parameters. Here, r corresponds to the three components of Euler vectors' rotation parameters on the coordinate axes. n stands for the number of stations.

The fitting results of the three approaches are tabulated in Table 1, accompanied by the presentation of residual velocity maps and detailed strain maps obtained using robust estimation RELSM. Figures 3 to Figure 5 illustrate the velocity residuals after fitting for the three approaches, while Figure 6 showcases the anomalous stations identified through robust RELSM selection. Additionally, Figure 7 depicts a detailed strain map of the Ordos and its neighboring areas, computed through fitting and calculation of velocity field data post-filtering using robust RELSM and visualized through computer visualization operations. Figures 1, Figure 2, Figure 6 and Figure 7 were drawn by GMT software, and Figures 3, Figure 4 and Figure 5 were drawn by MATLAB data processing platform.

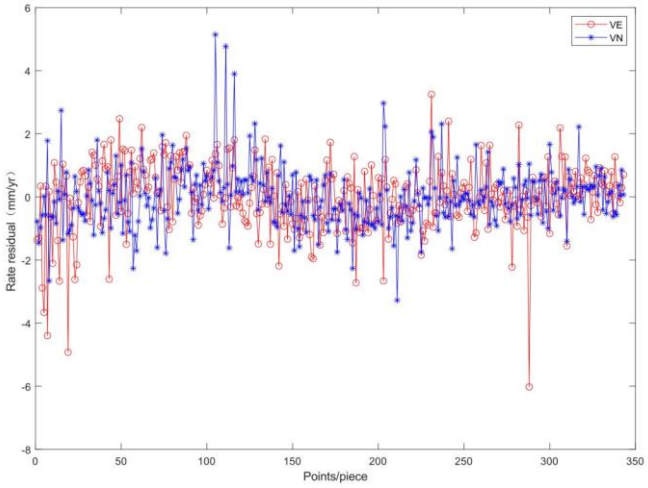

Figure 3 Approach I RELSM velocity residuals

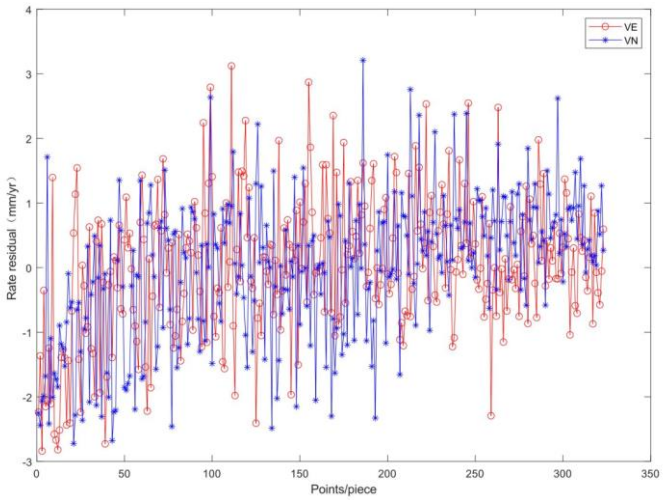

Figure 4 Residual velocities of the RRM model with robust estimation in Scheme 2

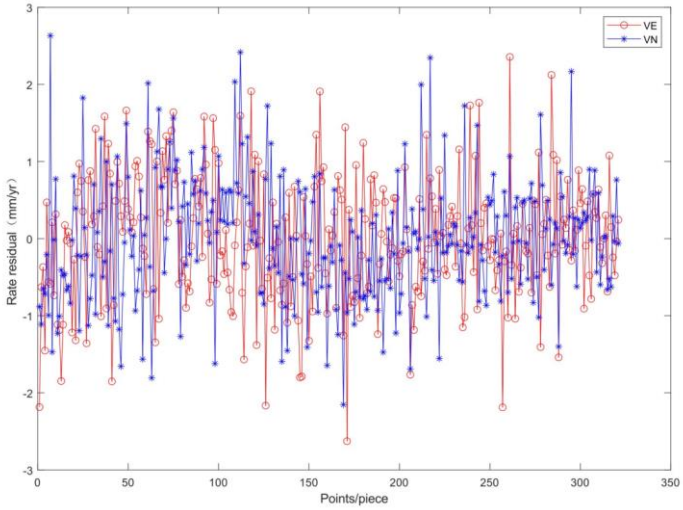

Figure 5 Residual velocities of the RELSM model with robust estimation in Scheme 3

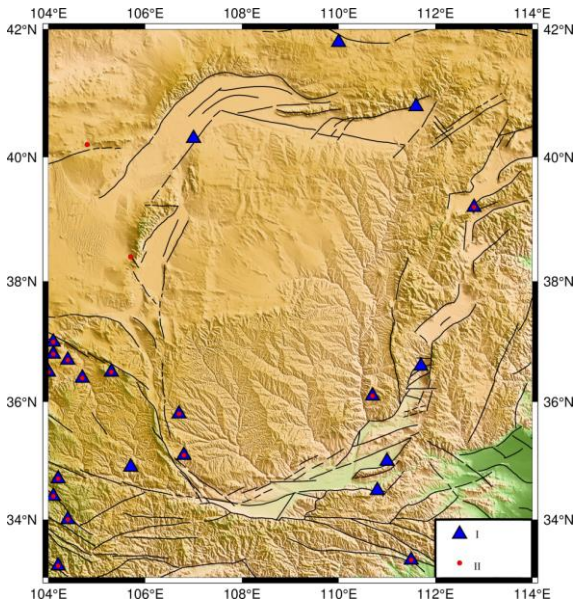

Figure 6 Anomalous stations

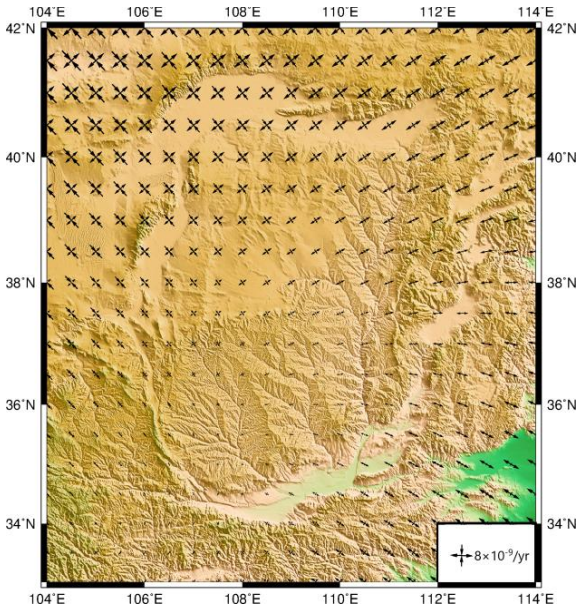

Figure 7 Strain field of Ordos and adjacent areas.

Table 1 Euler motion parameters and velocity residuals.

Approach	Anomalous Station Count	Euler Parameters			Velocity Residual Standard Deviation $S_{\Delta V}$ (mm/yr)
		l/(°)	ϕ/(°)	ω/((°)□Myr^{-1})	
I	–	42.395	72.338	0.087	1.009
II	17	49.106	70.432	0.094	0.840
III	22	48.619	70.840	0.093	0.787

From Figures 3 to 5, it can be observed that in Scheme I, the maximum residual velocity in the east-west direction exceeds 5mm/yr for certain stations, and in the north-south direction exceeds 6mm/yr. However, the majority of stations exhibit residual velocities distributed around 3mm/yr in both the east-west and north-south directions. In Scheme II, the maximum residual velocity does not exceed 4mm/yr in either the east-west or north-south directions. In Scheme III, the maximum residual velocity in both directions is within 3mm/yr, indicating that all three schemes consider the long-term trends of plate motion in their fits. Combining with Table 1, it can be seen that the standard deviations of the residual velocities for Scheme I, Scheme II, and Scheme III are 1.009mm/yr, 0.840mm/yr, and 0.787mm/yr respectively. This indicates that even with reasonable station selection using a rigid block motion model, excluding 17 anomalous stations and refitting, the accuracy still falls below that of fitting using the overall rotation and linear strain model of block motion. Scheme I, which uses RELSM, considers internal deformation but does not involve station selection, resulting in poor fitting. Scheme III, which considers internal deformation, employs a high breakdown rate robust estimation method to suppress outliers, conducts rigorous station selection by excluding 22 anomalous stations, and achieves the best fitting results.

From Figure 6, it is evident that the anomalous stations removed using robust estimation are distributed around various fault zones, primarily concentrated around the Haiyuan Fault Zone and the Shanxi Fault Zone. This suggests that the regions where anomalous stations are located are currently experiencing relatively active tectonic movement, deviating significantly from the overall trend of block motion. Using Scheme III to fit strain parameters and calculate detailed strain in the study area, overall, the principal compressive strain direction in the Ordos and adjacent areas is NE-SW, while the principal tensile strain direction is mainly NW-SE. Specifically, the western part of the Ordos block exhibits varying degrees of tension and compression, with directions close to N-S tension and W-S compression, showing a counterclockwise rotation. The deformation in the northeast part is primarily tensile, with a direction roughly NE-SW. Similarly, the deformation to the east of Ordos is predominantly tensile, with a direction approaching W-S. In the southern region of Ordos, represented by the Weihe River, the predominant strain trend is tension, with a direction trending towards W-S and slightly

deviating north-south. These results broadly align with those reported by Zhu. [19-20] regarding strain in the region, further illustrating the rationality of utilizing the iterative selection method based on the overall rotation and linear model of block motion (RELSM) with robust estimation for station selection, followed by RELSM velocity field fitting analysis of selected stations.

5. Conclusion

This article utilizes the overall rotation of the block and the robust estimation of linear models for iterative screening. The screened stations after iteration are subjected to RELSM velocity field fitting analysis, combined with computer visualization mapping. The results visually indicate that this method can take into account the smoothness of the motion of each point within the block (consistent with the overall rigid motion trend of the block) and irregular deformations caused by internal tectonic motion, i.e., taking into account the integrity and local differences of crustal motion. However, due to the assumption that the interior of the block is linearly deformed in RELSM, there are certain limitations in using the region, which may be difficult to apply in areas with complex geological structures. In addition, the data used in this article is only the referenced open-source velocity field data from 2009 to 2014, which is slightly insufficient in terms of accuracy, so the fitting effect may be biased from reality. However, overall, it does not affect the method becoming a reference method for regional station screening and fitting.

Acknowledgment

We would like to thank the Guizhou Province Youth Science and Technology Talent Growth Project (Qianjiaohe KY Zi [2022] 132, [2022] 135); Karst Plateau Resources and Environment Remote Sensing Talent Team (Bi Wei Ren Ling Tong [2023] No. 14); Smart Geospatial Information Application Engineering Center (Bike Union [2023] No. 8); First Class Professional Construction Project of Guizhou Engineering Applied Technology College (No. ZY202104); Provide corresponding financial support for projects such as the Guizhou Province Youth Science and Technology Talent Growth Project (Qianjiaohe KY Zi [2022] 133).

References

[1] Burbidge D R. Thin Plate Neotectonic Models of the Aus-tralian Plate. Journal of Geophysical Research: SolidEarth, 2004, 109(B10).

[2] Zhao Lihua, Yang Yuanxi, Wang Qingliang. Deformation analysis and fitting estimation model considering regional tectonic features. Acta Geodaetica et Cartographica Sinica, 2011, 40(4): 435-441.

[3] Lohman, R.B., and P. Zebker. Deformation of the Earth's Surface Due to Surface Loads: Representation in Terms of Multipoles. Journal of Geophysical Research: Solid Earth 2016.10, no. 3,762-795.

[4] Francesco Iezzi, Gerald Roberts,Joanna Faure Walker, Ioannis Papanikolaou, Athanassios Ganas, Georgios Deligiannakis, et al. Temporal and spatial earthquake clustering revealed through comparison of millennial strain-rates from 36Cl cosmogenic exposure dating and decadal GPS strain-rate .Scientific Report. 2021. 11: 23320.

[5] M. Radiguet, H. Perfettini, N. Cotte,A. Gualandi, B. Valette, V. Kostoglodov, et al. Triggering of the 2014 Mw7.3 Papanoa earthquake by a slow slip event in Guerrero, Mexico. 2016. 9. (3) 829-833.

[6] Zeyu Jin,Yuri Fialkol. Coseismic and Early Postseismic Deformation Due to the 2021 M7.4 Maduo (China) Earthquake. Geophysical Research Letters. 2021. 10. (21), 1-10.

[7] Han Yue, Jianbao Sun, Min Wang, Zhengkang Shen, Mingjia Li, Lian Xue, et al. The 2019 Ridgecrest, California earthquake sequence: Evolution of seismic and aseismic slip on an orthogonal fault system .2021. 9. (570): 117066.

[8] Laura M. Wallace, Yoshihiro Kaneko, Sigrún Hreinsdóttir, Ian Hamling, Zhigang Peng, Noel Bartlow, et al. Large-Scale Dynamic Triggering of Shallow Slow Slip Enhanced by Overlying Sediment Wedge. Nature Geoscience 2017. 10. 765-770.

[9] Yang Gao, HuRong Duan, YongZhi Zhang, JiaYing Chen, HeTing Jian, Rui Wu, et al. Joint Inversion of GNSS and InSAR Data for the 2019 Mw 6.4 and Mw 7.1 Ridgecrest, California, Earthquakes . Journal of Geophysical Research: Solid Earth 2021. 11: 14188.

[10] Toshihiro Igarashi, Aitaro Kato. Evolution of aseismic slip rate along plate boundary faults before and after megathrust earthquakes. 2021. 2(60): 1-6.

[11] Li Yanxing, Huang Cheng, Hu Xinkang. Rigid elastoplastic motion model of intra-plate blocks and strain state of major blocks in mainland China. Seismological Journal, 2001, 23(6): 565-572.

[12] Li Yanxing, Li Zhi, Zhang Jinghua. Horizontal strain field of mainland China and surrounding areas. Chinese Journal of Geophysics, 2004, 47(2): 222-231.

[13] Li Yaping, Sun Fuping, Zhu Xinhui. Application of robust principal component estimation in plate motion parameter calculation. Surveying and Mapping Engineering, 2016, 25(8): 38-41.
[14] Zhao Lihua. Research on the implementation of regional crustal motion model: Theory and method. Xi'an: Chang'an University, 2011.
[15] Yang Yuanxi. Theory and application of robust estimation. Beijing: August 1st Publishing House, 1993.
[16] Yongqi Z, Hongguang Z, Enhui Z. Study on effective elastic thickness of lithosphere and its tectonic significance in surrounding area of Ordos Block . Journal of Physics: Conference Series, 2023, 2621 (1): 1-12.
[17] Liu C, Ji L, Zhu L. Present-Day Three-Dimensional Deformation across the Ordos Block, China, Derived from InSAR, GPS, and Leveling Observations. Remote Sensing, 2023, 15 (11): 2-15.
[18] CUI D X, HAO M, LI Y H. Present-day crustal movement and strain of the surrounding area of Ordos block derived from repeated GPS observations. Chinese J. Geophys. 2016. 59(10): 3646-3661.
[19] Bin Z, Yong H, Caihong Z. Crustal deformation on the Chinese mainland during 1998-2014 based on GPS data. Geodesy and Geodynamics, 2015, 6 (01): 7-15.
[20] Zhu Shoubiao. Strain-Rates from GPS Measurements in the Ordos Block, China: Implications for Geodynamics and Seismic Hazards. Remote Sensing. 2022.14, no.3: 779.